Research Square

Preprints are preliminary reports that have not undergone peer review.
They should not be considered conclusive, used to inform clinical practice,
or referenced by the media as validated information.

Harnessing synergistic SN38/quercetin nanomicelles via inhalation for enhanced lung cancer treatment

Xudong Fan
Hangzhou Red Cross Hospital
Jingming Luo
Zhejiang Chinese Medical University
XiaoQian Tang
Zhejiang Chinese Medical University
Jie Zhang
Zhejiang Chinese Medical University
Ruoying Zhang
Hangzhou Red Cross Hospital
Xinjun Cai
zjtcmcxj@zcmu.edu.cn

Hangzhou Red Cross Hospital

Research Article

Keywords: lung cancer, SN38, quercetin, inhalation, nanomicelles

Posted Date: May 27th, 2026

DOI: https://doi.org/10.21203/rs.3.rs-9513069/v1

License: This work is licensed under a Creative Commons Attribution 4.0 International License.
Read Full License

Additional Declarations: No competing interests reported.

Version of Record: A version of this preprint was published at Drug Delivery and Translational Research on August 3rd, 2026. See the published version at https://doi.org/10.1007/s13346-026-02197-4.

Abstract

Lung cancer continues to be a major contributor to global cancer-related morbidity and mortality, with chemotherapeutic approaches such as irinotecan often limited by poor solubility, systemic toxicity, and multidrug resistance driven by P-glycoprotein (P-gp)-mediated efflux. To address these challenges, this study developed polymeric nanomicelles for the pulmonary co-delivery of SN38—the active metabolite of irinotecan—and quercetin, a natural flavonoid known to reverse P-gp-dependent resistance. The dual-drug-loaded nanomicelles (SN38/QU-PPM), prepared via nanoprecipitation, exhibited uniform morphology, colloidal stability, and pH-responsive drug release under acidic conditions. In vitro evaluations demonstrated enhanced cellular uptake, effective P-gp inhibition, and increased intracellular accumulation of SN38, leading to superior cytotoxicity against lung cancer cells compared to SN38 alone. In an orthotopic lung tumor model, nebulized administration resulted in significantly higher pulmonary SN38 levels and stronger tumor suppression relative to intravenous delivery, alongside evidence of promoted apoptosis and reduced proliferation in tumor tissues, without notable systemic toxicity. These findings indicate that nebulized co-delivery of SN38 and quercetin via polymeric nanomicelles offers a promising lung-targeted strategy that enhances local drug exposure, overcomes efflux-mediated resistance, and reduces off-target effects, supporting its potential clinical translation.

1. Introduction

Lung cancer remains one of the most common and lethal malignancies worldwide. In 2022, it accounted for approximately 2.48 million new cases and 1.8 million deaths—representing 12.4% of all new cancer diagnoses and 18.7% of cancer-related deaths, respectively [1, 2]. The first-line chemotherapy typically combines platinum-based agents with topoisomerase inhibitors [3]. However, these regimens are limited by two major issues. First, substantial toxicity—most notably nephrotoxicity, myelosuppression, and severe nausea and vomiting—restricts both drug selection and dosing. Second, although initial responses are often favorable, most patients ultimately develop drug resistance, leading to relapse, disease progression, and cross-resistance, which often requires modification of the therapeutic strategy [4–6].

Topoisomerase inhibitors, which induce cellular apoptosis by disrupting deoxyribonucleic acid (DNA) replication and repair, are widely used in lung cancer therapy [7]. Irinotecan, a semi-synthetic prodrug derived from camptothecin, is converted by hepatic carboxylesterases into the active metabolite SN38 [8]. Although SN38 exhibits significantly higher antitumor potency than its parent compound, its poor aqueous solubility and chemical instability limit direct clinical application. Consequently, formulation strategies have been developed to improve local concentration and pharmacokinetics [9]. For example, glycan-SN38 prodrugs enhance solubility and stability while enabling tumor-responsive release. Emerging delivery platforms—liposomes [10, 11], poly (lactic-co-glycolic acid) (PLGA) nanoparticles [12], and magnetic carriers such as silica or ferrite nanoparticles [13, 14]—can further increase SN38 bioavailability and enable tumor-targeted delivery, especially when combined with antibody conjugation or external magnetic guidance [15, 16].

Tumor chemoresistance arises from multiple molecular mechanisms—enhanced DNA repair, increased drug efflux, altered drug targets, and changes in the tumor microenvironment—all of which reduce the efficacy of chemotherapy [17]. P-glycoprotein (P-gp), an adenosine triphosphate (ATP)-dependent efflux transporter, is a key mediator of this resistance [18]. Many chemotherapeutic agents used clinically for lung cancer, including doxorubicin, vincristine, and paclitaxel, are known P-gp substrates [19, 20]. Studies have shown that lung cancer cells resistant to various chemotherapeutic agents frequently overexpress P-gp, and coadministration of P-gp inhibitors can substantially resensitize these cells to treatment [21, 22]. Moreover, as demonstrated by Noro et al. and Weng et al., antibody-drug conjugates that incorporate P-gp inhibitors and employ self-immolative linkers can effectively overcome multidrug resistance and have shown promising antitumor activity in resistant tumor models [16, 23]. Therefore, incorporating P-gp inhibitors into drug formulations may be a promising approach to overcoming chemoresistance.

Several P-gp inhibitors, including verapamil, cyclosporin A, and quinine, have been developed; however, most show limited specificity and significant systemic toxicity [24]. Quercetin, a natural flavonoid widely present in plants and dietary sources, has demonstrated antitumor effects in lung cancer through multiple mechanisms. Studies have shown that quercetin can induce apoptosis in lung cancer cells by upregulating pro-apoptotic proteins such as Bax and caspases and downregulating anti-apoptotic proteins like B-cell lymphoma 2 (Bcl-2), thereby disrupting tumor cell homeostasis and triggering programmed cell death [25, 26]. Moreover, quercetin suppresses proliferation, invasiveness, and chemoresistance by modulating key signaling pathways [27–30].

Building on these findings, multiple groups have developed nanoscale delivery systems to enhance quercetin's efficacy and overcome drug resistance. For example, Wang et al. prepared chitosan nanoparticles co-loading paclitaxel and quercetin and further functionalized them for active targeting of epidermal growth factor receptor (EGFR)-overexpressing lung cancer cells [31], while Tang et al. engineered silk fibroin nanoparticles grafted with Pluronic F127 to achieve superior mucus penetration [32]. Current quercetin nanoformulations range from traditional mixed micelles, chitosan nanoparticles, and nanocomposite microspheres to emerging platforms such as metal-organic frameworks and protein-based nanoparticles, each offering distinct advantages for delivery and tumor targeting [32–36]. Given quercetin's multifaceted antitumor actions—apoptosis induction, cell-cycle arrest, tumor microenvironment modulation, and reversal of drug resistance—nano-delivery can further enhance its therapeutic potential. Therefore, we explored incorporating quercetin as an adjuvant to inhibit drug efflux and delay resistance, emphasizing combination strategies, formulation optimization, and the rationale for inhalation administration in lung cancer therapy.

Enhancing efficacy while reducing toxicity can be achieved not only by optimizing drug combinations and dosage forms, but also by selecting administration routes suited to the disease. Nebulized inhalation therapy for lung cancer offers several advantages: (□) it directly targets the lungs, producing higher local drug concentrations at tumor sites while minimizing systemic exposure and sparing healthy tissues [37]; (□) it lowers systemic toxicity because the drug is retained in the lungs rather than circulating broadly—an important benefit for cytotoxic agents [38, 39]; (□) it bypasses first-pass hepatic metabolism,

improving bioavailability, simplifying formulations, and reducing hepatotoxicity risk [40, 41]; and (□) it enables tailored formulation design—particle size can be tuned to favor bronchial or deep-lung deposition, and controlled-release systems can sustain therapeutic pulmonary concentrations to prolong effect and reduce dosing frequency [42]. Overall, nebulized inhalation provides a safe, efficient, and targeted pulmonary delivery platform that enhances local therapeutic effects while limiting systemic side effects, making it a promising approach for lung cancer treatment.

Therefore, this study aimed to develop a synergistic therapeutic strategy by combining SN38 with quercetin, delivered via an acid-responsive nanoplatform for pulmonary administration to achieve targeted drug delivery to the lungs. Specifically, we constructed an SN38/quercetin@PEG-PMMSD nanomicelle (SN38/QU-PPM) acid-responsive nanoplatform, designed to enhance drug accumulation in lung tumor tissues and facilitate intracellular drug uptake within tumor cells, thereby improving the therapeutic efficacy against lung cancer. This approach is expected to increase the local concentration of SN38 in pulmonary tumors, elicit synergistic antitumor effects, and help overcome or delay the onset of multidrug resistance. Overall, this study provides a theoretical foundation and formulation rationale for the localized and precise treatment of lung cancer, and presents a potential strategy for repurposing conventional injectable chemotherapeutics through pulmonary delivery.

2. Materials and Methods

2.1. Materials

SN38, dimethyl sulfoxide (DMSO), indocyanine green (ICG), cyclosporin A (CsA) were purchased from Aladdin (Shanghai, China). Quercetin, pirarubicin (THP) were purchased from Shanghai Yien Chemical Technology Co., Ltd. (Shanghai, China). PEG-PMMSD was purchased from Xi'an ruixi Biological Technology Co., Ltd. (Xi'an, China). CCK-8 assay kit was obtained from Shanghai Liji Biotechnology Co., Ltd. (Shanghai, China). Dialysis membrane (MWCO: 14 kDa) was purchased from Beijing Labgic Technology Co., Ltd. (Beijing, China). Fetal bovine serum (FBS), DMEM, and hank's balanced salt solution (HBSS) buffer were obtained from Gibco (California, USA). 4,6-diamidino-2-phenylindole (DAPI), phosphate buffered saline (PBS) were acquired from Beyotime (Shanghai, China).

2.2. Preparation of SN38/QU-PPM

SN38/QU-PPM dual-loaded polymeric nanomicelles were prepared by a nanoprecipitation method with optimized formulation parameters. Briefly, 10 mg of PEG-PMMSD copolymer and 2 mg of drugs (SN38 and quercetin, mass ratio 1:1) were dissolved in 200 μL of DMSO. The solution was added dropwise into 1.8 mL of ultrapure water under magnetic stirring. After addition, the mixture was stirred in the dark for 1 h to allow micelle formation. Free drug and residual DMSO were removed by dialysis, affording the final nanomicelles.

For preparation of ICG-labeled fluorescent nanomicelles, SN38 was replaced with an equivalent mass of ICG and all other steps were performed as described above.

2.3. Characterization of SN38/QU-PPM

The physicochemical properties of the SN38/QU-PPM nanomicelles were comprehensively characterized. Hydrodynamic diameter, zeta potential and polydispersity index (PDI) were measured by dynamic light scattering (DLS) after dispersing the nanomicelles in ultrapure water. Morphology was investigated via transmission electron microscopy (TEM). For sample preparation, nanomicelle suspensions were drop-cast onto copper grids, negatively stained, air-dried, and subsequently imaged.

Drug loading (DL) and encapsulation efficiency (EE) were quantified by high-performance liquid chromatography (HPLC). Briefly, a known mass of drug-loaded nanomicelles was disrupted by mixing with acetonitrile and subjecting the mixture to ultrasonication to fully release SN38 and quercetin from the polymer matrix, followed by centrifugation to remove precipitated polymer and particulates. The clear supernatant was analyzed by HPLC; calibration curves were constructed from authentic SN38 and quercetin standards covering the expected concentration range and used to convert peak areas to concentrations. All samples and standards were prepared and analyzed in triplicate. DL and EE were calculated as follows:

DL (%) = (mass of drug encapsulated in nanomicelles / mass of drug-loaded nanomicelles) × 100

EE (%) = (mass of drug encapsulated in nanomicelles / mass of drug initially added during formulation) × 100

To assess the stability of nanomicelles over 7 days, the following protocol was performed: Nanomicelle suspensions were stored at 4°C throughout the study. At predetermined time intervals, the hydrodynamic particle size, zeta potential, and PDI were measured using DLS.

2.4. In vitro release test

The in vitro release profiles of SN38 and quercetin from the nanomicelles were evaluated using a dialysis technique across three distinct pH conditions: 7.4, 6.4, and 5.4. Throughout the experiment, samples were maintained at 37°C under continuous agitation. At predetermined intervals, aliquots were collected and analyzed via HPLC to determine drug concentration. The resulting data were plotted as cumulative release curves, enabling a clear assessment of the pH-responsive drug release behavior exhibited by the dual-drug loaded nanomicelles.

2.5. Cell uptake assay

Cellular uptake of nanomicelles was assessed in LLC-Luc cells by confocal laser scanning microscopy (CLSM). Fluorescent ICG-loaded nanomicelles (ICG-PPM and ICG/QU-PPM) were prepared and ICG content quantified by UV-Vis spectrophotometry to normalize dosing. LLC-Luc cells in log phase were seeded in confocal dishes at 1×10^5 cells/dish, allowed to adhere for 24 h, then treated with free ICG, ICG-PPM, or ICG/QU-PPM for 1, 2, or 4 h. After incubation, cells were washed three times with PBS, fixed

with 4% paraformaldehyde for 30 min, stained with DAPI for 10 min, washed a final time, suspended in 1 mL PBS, and imaged by CLSM.

2.6. Cytotoxicity test

The cytotoxicity of SN38/QU-PPM nanomicelles was evaluated using a CCK-8 assay. LLC-Luc cells in the logarithmic growth phase were seeded into 96-well plates at 1×10^4 cells per well and incubated for 24 h. Prior to treatment, the concentrations of SN38 and quercetin in the SN38/QU-PPM formulation were determined by HPLC and the working concentrations were adjusted to 600 ng/mL for SN38 and 800 ng/mL for quercetin; these values were used to standardize the dosing of all experimental groups. Cells were then treated with: control, blank nanomicelles (PPM), free quercetin (QU), free SN38, SN38-loaded nanomicelles (SN38-PPM), and dual-loaded nanomicelles (SN38/QU-PPM). After 24 h incubation, cell viability was measured according to the manufacturer's protocol.

2.7. Intracellular SN38 Quantification

Intracellular SN38 concentrations were measured by ultra-high-performance liquid chromatography coupled with tandem mass spectrometry (UHPLC-MS/MS) to evaluate nanomicelles delivery efficiency. Log-phase LLC-Luc cells were seeded at 5 × 105 cells/well in 6-well plates. After 24 h, cells were treated with free SN38, SN38-PPM, or SN38/QU-PPM (SN38 final concentration 0.5 μg/mL) and incubated for 1, 2, 4, or 6 h. At each time point, medium was removed, cells were washed three times with PBS, detached with trypsin, collected by centrifugation, and resuspended in PBS for counting. Cells were then lysed, lysates were centrifuged at 4°C, the supernatants were filtered through 0.22 μm membrane, and the filtrates were analyzed by UHPLC-MS/MS.

2.8. THP accumulation assay

To assess the inhibitory effect of quercetin on P-gp efflux, the intracellular accumulation of the P-gp fluorescent substrate THP was monitored. Log-phase LLC-Luc cells were seeded at a density of 1×10^4 cells per well in black opaque 96-well plates and incubated for 24 h. The culture medium was then removed, and the cells were washed with PBS prior to incubation with THP (2 μmol/mL) for 30 min. After three washes with PBS to eliminate extracellular THP, the cells were treated with the following groups: control (HBSS), positive control (CsA), free quercetin (QU), and quercetin-loaded nanomicelles (QU-PPM). All treatments were normalized to a quercetin-equivalent concentration of 5 μmol/mL and incubated at 37°C for 1, 2, 4, or 6 h. Following treatment, the cells were washed again, and 100 μL of HBSS was added to each well. Fluorescence was measured using a multifunction measuring instrument with excitation at 488 nm and emission at 570 nm.

For CLSM, LLC-Luc cells were seeded at a density of 1×10^5 cells per dish in confocal dishes and incubated for 24 h to allow attachment. The same treatment and washing procedures described above were then performed. After the final wash, 1 mL of HBSS was added to each dish, and intracellular fluorescence was immediately imaged using the CLSM to document both the localization and intensity of the fluorescence signal.

2.9. Establishment of orthotopic lung cancer model

Specific pathogen-free (SPF) grade male C57BL/6J mice (8 weeks old) were obtained from Shanghai Slake Experimental Animal Co., Ltd. (License No. SCXK [Shanghai] 2022-0004). Animals were housed in the Laboratory Animal Research Center of Zhejiang Chinese Medical University. All animal-related experiments were carried out in accordance with the guidance of the Zhejiang Chinese Medical University Animal Care and Use Committee (IACUC-20230227-02).

After 1 week of acclimatization, the mice were used to establish an orthotopic lung cancer model via direct intrathoracic injection of LLC-Luc cells. Following intraperitoneal anesthesia, a small incision was made, and 25 μL of cell suspension containing 5×10^5 LLC-Luc cells was injected into the left lung of each mouse. The incision was then closed with a surgical staple. One week after inoculation, successful establishment of the orthotopic lung cancer model was verified by an in vivo imaging system (IVIS), with obvious fluorescence signals observed in the lungs.

2.10. In vivo biodistribution

The biodistribution of nanomicelles was investigated in tumor-bearing mice using IVIS. The tumor-bearing mice were categorized into four groups: free ICG (inhalation), ICG-PPM (inhalation), ICG/QU-PPM (inhalation), and ICG/QU-PPM (intravenous) (n = 3). The ICG dose for all groups was 0.4 mg/kg. After anesthetizing the mice, the assigned drug was administered intratracheally using a nebulizer, while the ICG/QU-PPM intravenous group received the drug via tail vein injection. At 24 h post-dosing, mice were euthanized to collect fluorescence intensity signals from major tissues (heart, liver, spleen, tumor-bearing lung tissue, kidney) using IVIS.

To evaluate the in vivo distribution of SN38 delivered via different formulations and administration routes, tumor-bearing mice were randomly divided into four groups: free SN38 (inhalation), SN38-PPM (inhalation), SN38/QU-PPM (inhalation), and SN38/QU-PPM (intravenous). All mice received an SN38-equivalent dose of 4 mg/kg. At 24 h post-administration, the mice were euthanized, and samples of serum, heart, liver, spleen, lungs (including tumor tissue), and kidneys were collected. Each tissue was weighed, and an appropriate amount was first homogenized with ultrapure water, followed by the addition of an equal volume of acetonitrile. Homogenization was performed by adding 100 μL of grinding solution per 100 mg of tissue. Serum and tissue homogenates were centrifuged at 12,000 rpm for 10 min, and the supernatants were appropriately diluted and stored at 4°C until analysis. The concentration of SN38 in each sample was determined using UHPLC-MS/MS.

2.11. In vivo antitumor pharmacodynamic studies

To evaluate antitumor efficacy, tumor-bearing mice were randomly divided into five groups: control (inhalation), free SN38 (inhalation), SN38-PPM (inhalation), SN38/QU-PPM (inhalation), and SN38/QU-PPM (intravenous). Treatments were administered on days 2, 5, and 8, with SN38 at a dose of 0.5 mg/kg. At the end of the treatment cycle, the tumor-bearing lungs were removed, and tumor volume was calculated. Histological analyses were performed to assess tumor apoptosis and proliferation:

TUNEL/DAPI staining for apoptotic cells, and immunohistochemical staining for Ki-67 as a proliferation marker. Fluorescence images were captured using a fluorescence microscope and quantified with ImageJ according to standard procedures.

2.12. In vivo biosafety assessment

To assess the biosafety of SN38/QU-PPM, major organs (heart, liver, spleen, and kidneys) were harvested from each group of tumor-bearing mice after treatment, fixed and processed as paraffin sections for H&E staining to evaluate histopathological changes. Body weight was recorded throughout the treatment period to monitor systemic toxicity. At the end of study, serum samples were collected for biochemical assays of liver and kidney function. Together, these measures provided a preliminary evaluation of the formulation's safety profile.

2.13. Statistical analysis

All data were analyzed using GraphPad Prism version 9.5.1 and presented as mean ± standard deviation (SD). Statistical significance was set at $P < 0.05$ was considered as extreme significant.

3. Results

3.1.Preparation and characterization of SN38/QU-PPM

Nanomicelles were successfully prepared using the nanoprecipitation method (Fig. 1A), and a systematic characterization of their physicochemical properties was performed. Before preparing SN38 and QU-loaded nanomicelles, blank nanomicelles (PPM) and SN38-loaded nanomicelles (SN38-PPM) were also prepared; their average particle size, zeta potential, and PDI are listed in Table S1. The blank PPM exhibited the smallest average particle size (120.37 ± 16.24 nm), with a slight increase observed for SN38-PPM and SN38/QU-PPM. The blank PPM carried a negative surface charge (zeta potential − 16.49 ± 0.22 mV), and drug loading had a negligible effect on zeta potential across formulations. All samples displayed low PDI (≤ 0.119), indicating excellent dispersion. TEM images of SN38-PPM and SN38/QU-PPM are shown in Fig. 1B and 1C, respectively. Quantitative analysis showed that SN38/QU-PPM exhibited drug loading (DL) and encapsulation efficiency (EE) values of 8.17 ± 0.94% and 67.97 ± 4.04% for SN38, and 10.52 ± 0.81% and 69.77 ± 1.16% for QU, respectively.

To further assess the drug release behavior of SN38/QU-PPM nanomicelles, the in vitro release profiles of both agents were examined under different pH conditions using a dialysis method. As shown in Fig. 1D and 1E, the cumulative release rates of SN38 and quercetin after 24 h were only 17.09% and 17.36%, respectively, at pH 7.4. When the pH decreased to 6.4, the release rates increased to 37.11% and 45.05%, respectively, and further rose to 83.58% and 87.97% at pH 5.4. These results demonstrate that the dual-drug-loaded nanomicelles possess excellent pH-responsive release characteristics. The stability of PPM, SN38-PPM, and SN38/QU-PPM at 4°C was investigated via DLS. As shown in Fig. 1F-H, the average particle size, zeta potential, and PDI of the three preparations showed good stability when stored at 4°C for 7 days.

3.2.Cell uptake assay

Cellular uptake of various ICG-based fluorescent formulations in LLC-Luc cells was evaluated using CLSM. As shown in Fig. 2A, cells treated with ICG/QU-PPM exhibited stronger intracellular fluorescence signals than those treated with free ICG or ICG-PPM, and this enhancing effect became more pronounced with prolonged incubation time. Quantitative analysis of intracellular fluorescence further confirmed these observations. As illustrated in Fig. 2B, the cellular uptake efficiency of ICG/QU-PPM was significantly higher than that of ICG-PPM after 2 h and 4 h of incubation ($P < 0.05$), indicating that co-loading quercetin effectively promoted the endocytosis of nanomicelles by tumor cells.

3.3.Cytotoxicity test

The cytotoxicity of SN38/QU-PPM against LLC-Luc cells was assessed using the CCK-8 assay. As shown in Fig. 2C, blank nanomicelles without drug loading exhibited negligible cytotoxicity, confirming the excellent biocompatibility of the carrier. Treatment with free quercetin alone inhibited lung cancer cell viability by approximately 30%, reflecting its moderate but distinct antitumor activity ($P < 0.0001$). In contrast, SN38/QU-PPM demonstrated markedly higher cytotoxicity than both free SN38 and SN38-PPM ($P < 0.01$). These findings indicate that co-delivery of SN38 and quercetin via nanomicelles produces a synergistic inhibitory effect on tumor cell proliferation, likely due to improved cellular uptake and complementary pharmacological actions of the two agents.

3.4. THP accumulation assay

To evaluate the effect of quercetin on P-gp-mediated drug efflux, LLC-Luc cells were treated with pirarubicin (THP), a fluorescent P-gp substrate, and intracellular fluorescence was analyzed using confocal laser scanning microscopy. As shown in Fig. 3A, the fluorescence intensity in the control group decreased over time, indicating active drug efflux. In contrast, cells treated with cyclosporin A, a known P-gp inhibitor, exhibited increased intracellular fluorescence. Notably, the QU-PPM group displayed stronger fluorescence signals than the free quercetin group at all time points, suggesting that nanomicelle-encapsulated quercetin more effectively inhibits P-gp-mediated efflux.

Quantitative analysis of intracellular fluorescence using a multifunction measuring instrument further supported these findings. As illustrated in Fig. 3B, the fluorescence intensity in the QU-PPM group was significantly higher than that in the free quercetin group at all measured time points ($P < 0.01$). This suggests that micellar encapsulation enhances quercetin's ability to inhibit P-gp-mediated efflux and improves intracellular drug retention.

3.5. Intracellular SN38 Quantification

To assess quercetin's effect on intracellular SN38 delivery, LLC-Luc cells were treated with SN38-PPM or SN38/QU-PPM, and intracellular drug concentrations were quantified at multiple time points. As shown in Fig. 3C, intracellular SN38 accumulation increased in a time-dependent manner for both formulations. Notably, the SN38/QU-PPM group exhibited significantly higher intracellular SN38 levels than the

SN38-PPM group from 2 h onward ($P < 0.05$), indicating that quercetin enhances cellular uptake and retention of SN38.

3.6. In vivo biodistribution

To further investigate the biodistribution of dual-drug-loaded nanomicelles, major organs were harvested 24 h post-administration and subjected to ex vivo fluorescence imaging. As displayed in Fig. 4A, the ICG signal in the free ICG (inhalation) group was almost completely cleared. In contrast, nanomicelle formulations exhibited stronger residual fluorescence, especially in the lungs. Notably, inhaled ICG-PPM and ICG/QU-PPM showed prominent accumulation in lung tissue, whereas intravenous administration of ICG/QU-PPM resulted in widespread distribution, with the highest signal intensity detected in the liver. Quantitative analysis of fluorescence intensity in the excised organs further validated these findings. As shown in Fig. 4B, the inhalation groups exhibited significantly higher drug accumulation in the lungs compared with the intravenous group, accompanied by markedly lower signals in the liver and kidney. Collectively, these results demonstrate that pulmonary administration of nanomicelles facilitates lung-targeted delivery while reducing off-target distribution, thus presenting distinct advantages for localized lung cancer therapy.

To evaluate the distribution profile of SN38 via different administration routes, tumor-bearing mice were sacrificed 24 h post-treatment, and SN38 concentrations in various tissues were quantified. As depicted in Figure S1, the SN38/QU-PPM (inhalation) group achieved the highest pulmonary drug concentration, at 183.17 ± 9.39 ng/mg, which was significantly higher than that in all other groups ($P < 0.01$). In contrast, the SN38/QU-PPM (intravenous) group showed the most prominent hepatic accumulation (247.53 ± 7.54 ng/mg), whereas all inhalation groups maintained liver SN38 levels below 70 ng/mg. Serum SN38 concentrations in the inhalation groups remained below 32 ng/mL, while the intravenous group exhibited an average level of 43.47 ± 6.53 ng/mL. Notably, pulmonary SN38 levels in the SN38/QU-PPM (inhalation) group were 3.33-fold higher than those in the intravenous group, and its hepatic concentration was reduced to merely 14.56% of the intravenous level.

3.7. In vivo antitumor pharmacodynamic studies

To assess the in vivo antitumor efficacy of SN38/QU-PPM, mice bearing orthotopic lung tumors were treated with various formulations by aerosol inhalation or intravenous injection. Tumor progression was monitored by serial bioluminescence imaging. As shown in Fig. 5A, luminescent tumor signals decreased progressively in the treatment groups, with the SN38/QU-PPM inhalation group showing the most pronounced signal suppression by day 7, indicating superior inhibition of tumor growth. Gross examination of the excised lungs further confirmed the therapeutic benefit of inhaled dual-drug-loaded nanomicelles. As shown in Fig. 5B, the SN38/QU-PPM (inhalation) group exhibited a markedly reduced tumor burden compared with all other groups. Quantitative analysis (Fig. 5C) revealed that this group had the smallest mean tumor volume and the highest tumor growth inhibition rate. Histological analysis of tumor sections was performed to evaluate cellular proliferation and apoptosis. Ki-67 immunostaining

showed a pronounced reduction in proliferative activity in tumors from the SN38/QU-PPM (inhalation) group, whereas TUNEL staining revealed a substantial increase in apoptotic cells (Fig. 5D). Quantification of these markers (Figure S2) confirmed the immunohistochemical observations, supporting the enhanced antiproliferative and pro-apoptotic effects of the inhaled dual-drug formulation. Collectively, these results indicate that inhaled SN38/QU-PPM effectively suppresses tumor cell growth and promotes apoptosis in vivo.

3.8. In vivo biosafety assessment

During the 11-day treatment period, all treatment groups exhibited significant body weight loss relative to the control group, with the inhalation SN38/QU-PPM and SN38/QU-PPM (i.v.) groups showing the most pronounced reductions (Figure S3). Histopathological analysis via H&E staining revealed no obvious structural damage or pathological lesions in the major organs across all groups (Figure S4). Further serum biochemical testing confirmed that no significant hepatotoxicity occurred in any treatment arm, as evidenced by unaltered alanine aminotransferase (ALT) and aspartate aminotransferase (AST) levels; however, intravenous administration of SN38/QU-PPM induced severe renal dysfunction, marked by significantly elevated blood urea nitrogen (BUN) and creatinine (CREA) levels (Figure S5).

4. Discussion

PEG-PMMSD is an amphiphilic block copolymer composed of a PEG hydrophilic segment and a 5-methyl-5-methacryloyloxy-methyl-2-styrenyl-[1, 3]-dioxane hydrophobic block, synthesized via polymerization of the MMSD monomer, wherein the styryl-substituted dioxane acetal structure confers pH-responsive properties to the resulting polymeric micelles. This amphiphilic block copolymer spontaneously self-assembles into nanomicelles in aqueous environments, forming a hydrophobic inner core suitable for encapsulating poorly water-soluble drugs such as SN38 and quercetin, while the hydrophilic outer shell ensures colloidal stability and biocompatibility [43]. The resulting nanomicelles exhibited pH-responsive drug release profiles, with accelerated release under acidic conditions (pH 5.4) compared to neutral pH (7.4), attributable to the acid-sensitive backbone structure of PEG-PMMSD and its relevance to the mildly acidic tumor microenvironment. Notably, quercetin released faster than SN38 under identical conditions, potentially due to differences in molecular weight and carrier affinity. Various pH-responsive mechanisms—such as acid-triggered bond cleavage, pH-driven conformational changes, and differential swelling—have been explored in nanocarrier systems [44, 45], offering valuable references for the rational design of inhalable smart delivery systems tailored to the tumor microenvironment.

In vitro cytotoxicity assays revealed that SN38/QU-PPM exhibited significantly enhanced antiproliferative activity against LLC-Luc cells compared to SN38-PPM alone. This enhanced efficacy is attributed to the combined action of the nanocarrier and quercetin. Fluorescence imaging revealed that, compared to free ICG, the intracellular fluorescence intensity was markedly higher in the ICG-PPM and ICG/QU-PPM groups, largely attributable to enhanced cellular uptake facilitated by the nanomicelles, which was

further amplified in the presence of quercetin. In addition, quercetin inhibited P-gp-mediated efflux, as demonstrated by increased intracellular retention of the P-gp substrate THP. These findings suggest that quercetin not only promotes the cellular uptake of nanocarriers, but also counteracts P-gp-associated multidrug resistance. Beyond functional inhibition, quercetin has been reported to modulate P-gp expression via multiple signaling pathways (e.g., PI3K/Akt, FZD7/β-catenin) [46, 47] and to directly interfere with P-gp function by binding near the nucleotide-binding domain and inhibiting ATPase activity [48]. Collectively, these mechanistic insights support the rational co-delivery of quercetin with chemotherapeutics to enhance drug retention and overcome multidrug resistance.

In vivo biodistribution studies demonstrated that nebulization notably enhanced the pulmonary accumulation of SN38: the nebulized SN38/QU-PPM group exhibited approximately 3.3-fold higher lung concentrations compared with the intravenous injection group. This improvement was accompanied by reduced drug distribution in the liver and kidneys, which can be ascribed to the advantages of inhalation administration and the favorable physicochemical properties of the nanomicellar formulation. In an orthotopic lung tumor model, nebulized SN38/QU-PPM exerted the most potent inhibitory effect on tumor growth, as verified by bioluminescence imaging, tumor volume measurement, TUNEL assay, and Ki-67 staining. These results indicate that the nebulized formulation effectively induces tumor cell apoptosis and suppresses tumor proliferation in vivo. Notably, the formulation exhibited good biosafety when administered via nebulized inhalation. Although a decrease in body weight was observed in mice during the treatment period, their liver and kidney function indicators remained normal, and no histopathological damage was found in major organs. However, a limitation of the current study is that the whole-lung biodistribution data failed to distinguish drug distribution between tumor tissues and normal lung parenchyma; therefore, further imaging studies are required to clarify the intratumoral localization of the drug.

This study still has some limitations. The employed LLC-luc tumor model does not represent P-gp-overexpressing multidrug-resistant phenotypes; thus, the resistance-reversal effect of quercetin in clinically relevant chemoresistant lung cancer remains to be verified using resistant cell lines such as A549/DOX or LLC/ADR. Compared with other inhalable delivery systems, our SN38/QU-PPM exhibits good safety and pulmonary deposition but lacks sustained-release and active targeting functions. Inhalation therapy is effective for local tumors but limited in patients with distant or metastatic lesions, and balancing local and systemic exposure remains challenging. From a translational perspective, this inhalable formulation is more suitable for central non-small cell lung cancer and overcomes the low bioavailability of quercetin by synchronous pulmonary delivery, prolonging local retention and improving therapeutic overlap. In summary, we developed an inhalable dual-drug nanomicelle system for co-delivering SN38 and quercetin, which significantly enhanced pulmonary drug accumulation and antitumor efficacy via inhibiting P-gp-mediated efflux. Despite limitations including the need for improved biodistribution evaluation and validation in chemoresistant models, this platform represents a promising strategy for localized lung cancer therapy. Future studies will focus on pharmacokinetic optimization and translational research for wider clinical application.

5. Conclusions

This study developed a dual-drug PEG-PMMSD nanomicellar formulation (SN38/QU-PPM) for the inhalation delivery of SN38 and quercetin. The formulation exhibited favorable physicochemical characteristics, including a monodisperse particle size, robust encapsulation efficiency, and good stability, as well as a pH-responsive drug release profile in acidic environments. In vitro, quercetin inhibited P-gp–mediated efflux, thereby increasing intracellular accumulation and potentiating SN38 cytotoxicity in lung cancer cells. In an orthotopic lung tumor model, nebulized SN38/QU-PPM markedly enhanced pulmonary deposition and tumor-directed delivery relative to free drug and intravenous administration, translating into superior antitumor efficacy, while exhibiting an acceptable safety profile with no significant systemic toxicity. Collectively, these results indicate that inhalable co-delivery of SN38 and quercetin via nanomicelles is a promising strategy to improve the therapeutic index of lung cancer chemotherapy by increasing local drug concentration, overcoming drug resistance, and reducing off-target effects, and they provide a rationale for further development of inhalation-based nanomedicine platforms for respiratory malignancies.

Abbreviations

P-gp	P-glycoprotein
DNA	Deoxyribonucleic acid
PLGA	Poly (lactic-co-glycolic acid)
ATP	Adenosine triphosphate
Bcl-2	B-cell lymphoma 2
EGFR	epidermal growth factor receptor
DMSO	dimethyl sulfoxide
ICG	Indocyanine green
CsA	Cyclosporin A
THP	Pirarubicin
FBS	Fetal bovine serum
HBSS	Hank's balanced salt solution
DAPI	4,6-diamidino-2-phenylindole
PBS	Phosphate buffered saline
PDI	Polydispersity index
DLS	Dynamic light scattering
TEM	Transmission electron microscopy
DL	Drug loading
EE	Encapsulation efficiency
HPLC	High-performance liquid chromatography
CLSM	Confocal laser scanning microscopy
UHPLC-MS/MS	Ultra-high-performance liquid chromatography coupled with tandem mass spectrometry
SPF	Specific pathogen-free
IVIS	In vivo imaging system
SD	Standard deviation
ALT	Alanine aminotransferase
AST	Aspartate aminotransferase
BUN	Blood urea nitrogen

CREA	Creatinine

Declarations

Supplementary Materials: The online version contains supplementary material available at

Author Contributions: Conceptualization, X.F. and J.L.; methodology, X.F. and J.L.; software, X.F., J.L. and X.T.; validation, X.F., J.L. and X.T.; formal analysis, X.F., J.L., X.T. and J.Z.; investigation, X.F., J.L., X.T. and J.Z.; resources, X.F., J.L., X.T. and J.Z.; data curation, X.F., J.L., X.T. and J.Z.; writing—original draft preparation, X.F., J.L. and X.T.; writing—review and editing, X.C. and R.Z.; visualization, X.F. and J.L.; supervision, X.F. and J.L.; project administration, R.Z. and X.C.; funding acquisition, R.Z. and X.C. All authors have read and agreed to the published version of the manuscript.

Funding: This research was funded by the Hangzhou Medical and Health Science and Technology Project (A20250256).

Institutional Review Board Statement: This research was approved by the Zhejiang Chinese Medical University Animal Care and Use Committee (IACUC-20230227-02).

Data Availability Statement: Data supporting the findings of this study are obtainable from the corresponding author upon justified request.

Conflicts of Interest: The authors declare no conflicts of interest.

References

1. J Zhou, Y Xu, J Liu, L Feng, J Yu, D Chen. Global burden of lung cancer in 2022 and projections to 2050: Incidence and mortality estimates from GLOBOCAN. Cancer Epidemiol. 2024;93:102693. https://doi.org/10.1016/j.canep.2024.102693.
2. F Bray, M Laversanne, H Sung, J Ferlay, R L Siegel, I Soerjomataram, A Jemal. Global cancer statistics 2022: GLOBOCAN estimates of incidence and mortality worldwide for 36 cancers in 185 countries. CA Cancer J Clin. 2024;74(3):229-63. https://doi.org/10.3322/caac.21834.
3. M Wang, R S Herbst, C Boshoff. Toward personalized treatment approaches for non-small-cell lung cancer. Nat Med. 2021;27(8):1345-56. https://doi.org/10.1038/s41591-021-01450-2.
4. K Gokduman. Strategies Targeting DNA Topoisomerase I in Cancer Chemotherapy: Camptothecins, Nanocarriers for Camptothecins, Organic Non-Camptothecin Compounds and Metal Complexes. Curr Drug Targets. 2016;17(16):1928-39. https://doi.org/10.2174/1389450117666160502151707.
5. M Molinaro, D Skrodzki, D Pan. Chemoradiotherapy and nanomedicine: Drug mechanisms and delivery systems. Wiley Interdiscip Rev Nanomed Nanobiotechnol. 2024;16(4):e1984. https://doi.org/10.1002/wnan.1984.

6. G Shen, S Li, Y Zhu, Z Xu, X Liu, C Lv, Z Xing, L Cui, W Li. Recent progress in topoisomerase inhibitors as anticancer agents: Research and design strategies for Topo I and II inhibitors via structural optimization. Bioorg Chem. 2025;165:109040. https://doi.org/10.1016/j.bioorg.2025.109040.
7. J Y Jang, D Kim, E Im, N D Kim. Etoposide as a Key Therapeutic Agent in Lung Cancer: Mechanisms, Efficacy, and Emerging Strategies. Int J Mol Sci. 2025;26(2). https://doi.org/10.3390/ijms26020796.
8. Q R Qi, H Tian, B S Yue, B T Zhai, F Zhao. Research Progress of SN38 Drug Delivery System in Cancer Treatment. Int J Nanomedicine. 2024;19:945-64. https://doi.org/10.2147/ijn.S435407.
9. X Y Yang, H Y Zhao, H Lei, B Yuan, S Mao, M Xin, S Q Zhang. Synthesis and Biological Evaluation of 10-Substituted Camptothecin Derivatives with Improved Water Solubility and Activity. ChemMedChem. 2021;16(6):1000-10. https://doi.org/10.1002/cmdc.202000753.
10. G Milano, F Innocenti, H Minami. Liposomal irinotecan (Onivyde): Exemplifying the benefits of nanotherapeutic drugs. Cancer Sci. 2022;113(7):2224-31. https://doi.org/10.1111/cas.15377.
11. Z Su, L Li, F Hao, J Zhao, M Li, X Zhao, D Zhao. A Stable Irinotecan Liposome with Enhanced Antitumor Activity in a Range of Tumor Models. Pharm Res. 2023;40(12):3043-58. https://doi.org/10.1007/s11095-023-03622-w.
12. F B Arslan, K Öztürk, E Tavukçuoğlu, S C Öztürk, G Esendağlı, S Çalış. A novel combination for the treatment of small cell lung cancer: Active targeted irinotecan and stattic co-loaded PLGA nanoparticles. Int J Pharm. 2023;632:122573. https://doi.org/10.1016/j.ijpharm.2022.122573.
13. D García-Soriano, P Milán-Rois, N Lafuente-Gómez, C Rodríguez-Díaz, C Navío, Á Somoza, G Salas. Multicore iron oxide nanoparticles for magnetic hyperthermia and combination therapy against cancer cells. J Colloid Interface Sci. 2024;670:73-85. https://doi.org/10.1016/j.jcis.2024.05.046.
14. C Chircov, M C Petcu, B S Vasile, B Purcăreanu, A I Nicoară, O C Oprea, R C Popescu. Irinotecan-loaded magnetite-silica core-shell systems for colorectal cancer treatment. Int J Pharm. 2024;661:124420. https://doi.org/10.1016/j.ijpharm.2024.124420.
15. F Gao, J Guo, S Liu, F Zhang, Y Zhang, L Wang. Empowering hydrophobic anticancer drugs by ultrashort peptides: General Co-assembly strategy for improved solubility, targeted efficacy, and clinical application. J Colloid Interface Sci. 2024;667:119-27. https://doi.org/10.1016/j.jcis.2024.04.013.
16. W Weng, T Meng, Q Zhao, Y Shen, G Fu, J Shi, Y Zhang, Z Wang, M Wang, R Pan, L Ma, C Chen, L Wang, B Zhou, H Zhang, J Pu, J Zhang, Y P Hu, G Hua, Y Qian, S H Liu, W Hu, X Meng. Antibody-Exatecan Conjugates with a Novel Self-immolative Moiety Overcome Resistance in Colon and Lung Cancer. Cancer Discov. 2023;13(4):950-73. https://doi.org/10.1158/2159-8290.Cd-22-1368.
17. S Boumahdi, F J de Sauvage. The great escape: tumour cell plasticity in resistance to targeted therapy. Nat Rev Drug Discov. 2020;19(1):39-56. https://doi.org/10.1038/s41573-019-0044-1.
18. J Sui, M He, Y Yang, M Ma, Z Guo, M Zhao, J Liang, Y Sun, Y Fan, X Zhang. Reversing P-Glycoprotein-Associated Multidrug Resistance of Breast Cancer by Targeted Acid-Cleavable Polysaccharide Nanoparticles with Lapatinib Sensitization. ACS Appl Mater Interfaces. 2020;12(46):51198-211. https://doi.org/10.1021/acsami.0c13986.

19. C Pi, W Zhao, M Zeng, J Yuan, H Shen, K Li, Z Su, Z Liu, J Wen, X Song, R J Lee, Y Wei, L Zhao. Anti-lung cancer effect of paclitaxel solid lipid nanoparticles delivery system with curcumin as co-loading partner in vitro and in vivo. Drug Deliv. 2022;29(1):1878-91. https://doi.org/10.1080/10717544.2022.2086938.
20. S Dallavalle, V Dobričić, L Lazzarato, E Gazzano, M Machuqueiro, I Pajeva, I Tsakovska, N Zidar, R Fruttero. Improvement of conventional anti-cancer drugs as new tools against multidrug resistant tumors. Drug Resist Updat. 2020;50:100682. https://doi.org/10.1016/j.drup.2020.100682.
21. S Özkaya Gül, B Şimşek, F Yıldız, E Aydemir. Cytotoxic Effect of Escitalopram/Etoposide Combination on Etoposide-Resistant Lung Cancer. Pharmaceuticals (Basel). 2025;18(4). https://doi.org/10.3390/ph18040531.
22. W Liu, X Zhang, H Sunakawa, L M B Perera, L Martha, K Mizoi, T Ogihara. Mechanism of Induction of P-gp Activity During MET Induced by DEX in Lung Cancer Cell Line. J Pharm Sci. 2024;113(6):1674-81. https://doi.org/10.1016/j.xphs.2024.02.027.
23. M Omori, R Noro, M Seike, K Matsuda, M Hirao, A Fukuizumi, N Takano, A Miyanaga, A Gemma. Inhibitors of ABCB1 and ABCG2 overcame resistance to topoisomerase inhibitors in small cell lung cancer. Thorac Cancer. 2022;13(15):2142-51. https://doi.org/10.1111/1759-7714.14527.
24. R W Robey, K M Pluchino, M D Hall, A T Fojo, S E Bates, M M Gottesman. Revisiting the role of ABC transporters in multidrug-resistant cancer. Nat Rev Cancer. 2018;18(7):452-64. https://doi.org/10.1038/s41568-018-0005-8.
25. S Alam, T Mohammad, R A Padder, M I Hassan, M Husain. Thymoquinone and quercetin induce enhanced apoptosis in non-small cell lung cancer in combination through the Bax/Bcl2 cascade. J Cell Biochem. 2022;123(2):259-74. https://doi.org/10.1002/jcb.30162.
26. P Yang, X Li, Q Wen, X Zhao. Quercetin attenuates the proliferation of arsenic-related lung cancer cells via a caspase-dependent DNA damage signaling. Mol Carcinog. 2022;61(7):655-63. https://doi.org/10.1002/mc.23408.
27. N Lotfi, Z Yousefi, M Golabi, P Khalilian, B Ghezelbash, M Montazeri, M H Shams, P Z Baghbadorani, N Eskandari. The potential anti-cancer effects of quercetin on blood, prostate and lung cancers: An update. Front Immunol. 2023;14:1077531. https://doi.org/10.3389/fimmu.2023.1077531.
28. W J Chen, J H Tsai, L S Hsu, C L Lin, H M Hong, M H Pan. Quercetin blocks the aggressive phenotype of triple-negative breast cancer by inhibiting IGF1/IGF1R-mediated EMT program. J Food Drug Anal. 2021;29(1):98-112. https://doi.org/10.38212/2224-6614.3090.
29. M Yousefi Zardak, F Keshavarz, A Mahyaei, M Gholami, F S Moosavi, E Abbasloo, F Abdollahi, M Hossein Rezaei, E Madadizadeh, N Soltani, F Bejeshk, N Salehi, F Rostamabadi, F Bagheri, M Jafaraghae, M Ranjbar Zeydabadi, M Baghgoli, G Sepehri, M A Bejeshk. Quercetin as a therapeutic agent activate the Nrf2/Keap1 pathway to alleviate lung ischemia-reperfusion injury. Sci Rep. 2024;14(1):23074. https://doi.org/10.1038/s41598-024-73075-7.
30. B Zhou, Y Yang, X Pang, J Shi, T Jiang, X Zheng. Quercetin inhibits DNA damage responses to induce apoptosis via SIRT5/PI3K/AKT pathway in non-small cell lung cancer. Biomed Pharmacother.

2023;165:115071. https://doi.org/10.1016/j.biopha.2023.115071.

31. Y Wang, H Yu, S Wang, C Gai, X Cui, Z Xu, W Li, W Zhang. Targeted delivery of quercetin by nanoparticles based on chitosan sensitizing paclitaxel-resistant lung cancer cells to paclitaxel. Mater Sci Eng C Mater Biol Appl. 2021;119:111442. https://doi.org/10.1016/j.msec.2020.111442.
32. Y Tang, L Zhang, R Sun, B Luo, Y Zhou, Y Zhang, Y Liang, B Xiao, C Wang. Pulmonary delivery of mucus-traversing PF127-modified silk fibroin nanoparticles loading with quercetin for lung cancer therapy. Asian J Pharm Sci. 2023;18(4):100833. https://doi.org/10.1016/j.ajps.2023.100833.
33. K Li, X Zang, X Meng, Y Li, Y Xie, X Chen. Targeted delivery of quercetin by biotinylated mixed micelles for non-small cell lung cancer treatment. Drug Deliv. 2022;29(1):970-85. https://doi.org/10.1080/10717544.2022.2055225.
34. M K Lawson. Improvement of Therapeutic Value of Quercetin with Chitosan Nanoparticle Delivery Systems and Potential Applications. Int J Mol Sci. 2023;24(4). https://doi.org/10.3390/ijms24043293.
35. X Cui, F Zhang, Y Zhao, P Li, T Wang, Z Xu, J Zhang, W Zhang. A novel ligand-modified nanocomposite microparticles improved efficiency of quercetin and paclitaxel delivery in the non-small cell lung cancer. Drug Deliv. 2022;29(1):3123-33. https://doi.org/10.1080/10717544.2022.2120567.
36. J Liu, C Liu, J Tang, Q Chen, Y Yu, Y Dong, J Hao, W Wu. Synergistic cerium oxide nanozymes: targeting DNA damage and alleviating tumor hypoxia for improved NSCLC radiotherapy efficiency. J Nanobiotechnology. 2024;22(1):25. https://doi.org/10.1186/s12951-023-02196-4.
37. Q Fan, Z Li, J Yin, M Xie, M Cui, C Fan, L Wang, J Chao. Inhalable pH-responsive DNA tetrahedron nanoplatform for boosting anti-tumor immune responses against metastatic lung cancer. Biomaterials. 2023;301:122283. https://doi.org/10.1016/j.biomaterials.2023.122283.
38. P J Kuehl, C M Yingling, D Dubose, M Burke, D A Revelli, W Chen, W W Dye, S A Belinsky, M Tessema. Inhalation delivery dramatically improves the efficacy of topotecan for the treatment of local and distant lung cancer. Drug Deliv. 2021;28(1):767-75. https://doi.org/10.1080/10717544.2021.1912209.
39. W H Lee, C Y Loo, D Traini, P M Young. Development and Evaluation of Paclitaxel and Curcumin Dry Powder for Inhalation Lung Cancer Treatment. Pharmaceutics. 2020;13(1). https://doi.org/10.3390/pharmaceutics13010009.
40. Q Jin, W Zhu, J Zhu, J Zhu, J Shen, Z Liu, Y Yang, Q Chen. Nanoparticle-Mediated Delivery of Inhaled Immunotherapeutics for Treating Lung Metastasis. Adv Mater. 2021;33(7):e2007557. https://doi.org/10.1002/adma.202007557.
41. Y Liu, W N Crowe, L Wang, W J Petty, A A Habib, D Zhao. Aerosolized immunotherapeutic nanoparticle inhalation potentiates PD-L1 blockade for locally advanced lung cancer. Nano Res. 2023;16(4):5300-10. https://doi.org/10.1007/s12274-022-5205-6.
42. D Bardoliwala, A Javia, S Ghosh, A Misra, K Sawant. Formulation and clinical perspectives of inhalation-based nanocarrier delivery: a new archetype in lung cancer treatment. Ther Deliv.

2021;12(5):397-418. https://doi.org/10.4155/tde-2020-0101.

43. L Lin, G Wang, J Zhang, J Luo, X Fan, J Gao, X Cai. Intratracheal Administration of pH-Responsive Nanomicelles: A More Effective Strategy for Enhanced Intracellular Drug Delivery in Lung Cancer Treatment. Int J Nanomedicine. 2026;21:555824. https://doi.org/10.2147/ijn.S555824.
44. G Ak. Covalently coupling doxorubicin to polymeric nanoparticles as potential inhaler therapy: in vitro studies. Pharm Dev Technol. 2021;26(8):890-8. https://doi.org/10.1080/10837450.2021.1950187.
45. J Pang, X Chen, Z Lin, S Yao, W Wang, H Wu, W Xing, J Yang. Inhalable pH-responsive charge-reversal polymer-small interfering RNA polyplexes for directed gene therapy of anaplastic lymphoma kinase fusion-positive lung cancer. J Control Release. 2025;381:113644. https://doi.org/10.1016/j.jconrel.2025.113644.
46. G Zhao, S Xue. Mechanism of Quercetin as a Multidrug-resistant Reversing Compound in Oxaliplatin-resistant Gastric-cancer Cell Lines. Altern Ther Health Med. 2023;29(8):54-9.
47. Z Chen, C Huang, T Ma, L Jiang, L Tang, T Shi, S Zhang, L Zhang, P Zhu, J Li, A Shen. Reversal effect of quercetin on multidrug resistance via FZD7/β-catenin pathway in hepatocellular carcinoma cells. Phytomedicine. 2018;43:37-45. https://doi.org/10.1016/j.phymed.2018.03.040.
48. K Singh, R B Patil, V Patel, J Remenyik, T Hegedűs, K Goda. Synergistic Inhibitory Effect of Quercetin and Cyanidin-3O-Sophoroside on ABCB1. Int J Mol Sci. 2023;24(14). https://doi.org/10.3390/ijms241411341.

Figures

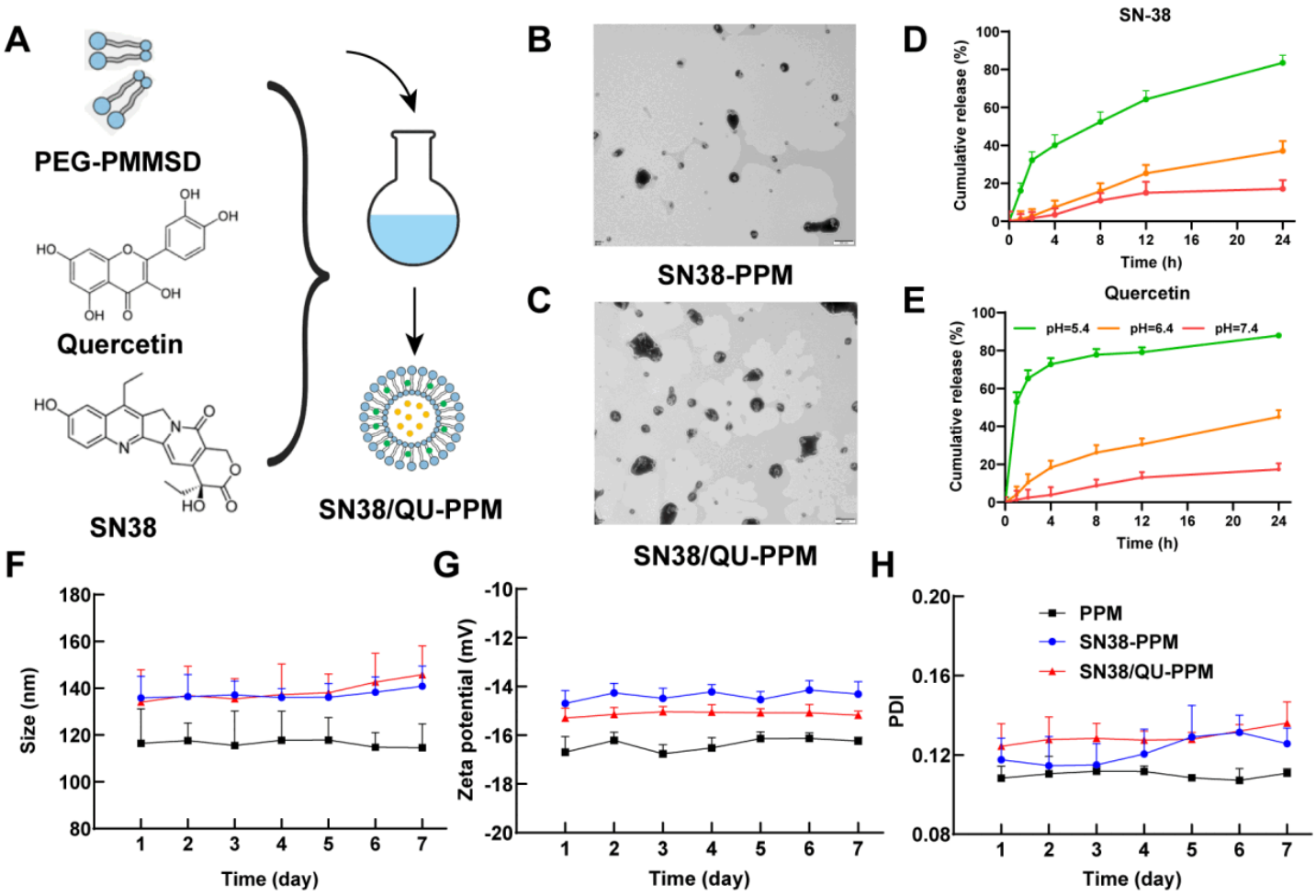


Figure 1

(A) Schematic illustration of SN38/QU-PPM preparation. (B, C) TEM images of SN38-PPM and SN38/QU-PPM. Scale bar: 500 nm. (D, E) Cumulative release of SN-38 or quercetin from SN38/QU-PPM at various conditions (pH 7.4, 6.4 or 5.4). (F-H) The stability of PPM, SN38-PPM, and SN38/QU-PPM in 4°C for 7 days (n = 3, mean ± SD).

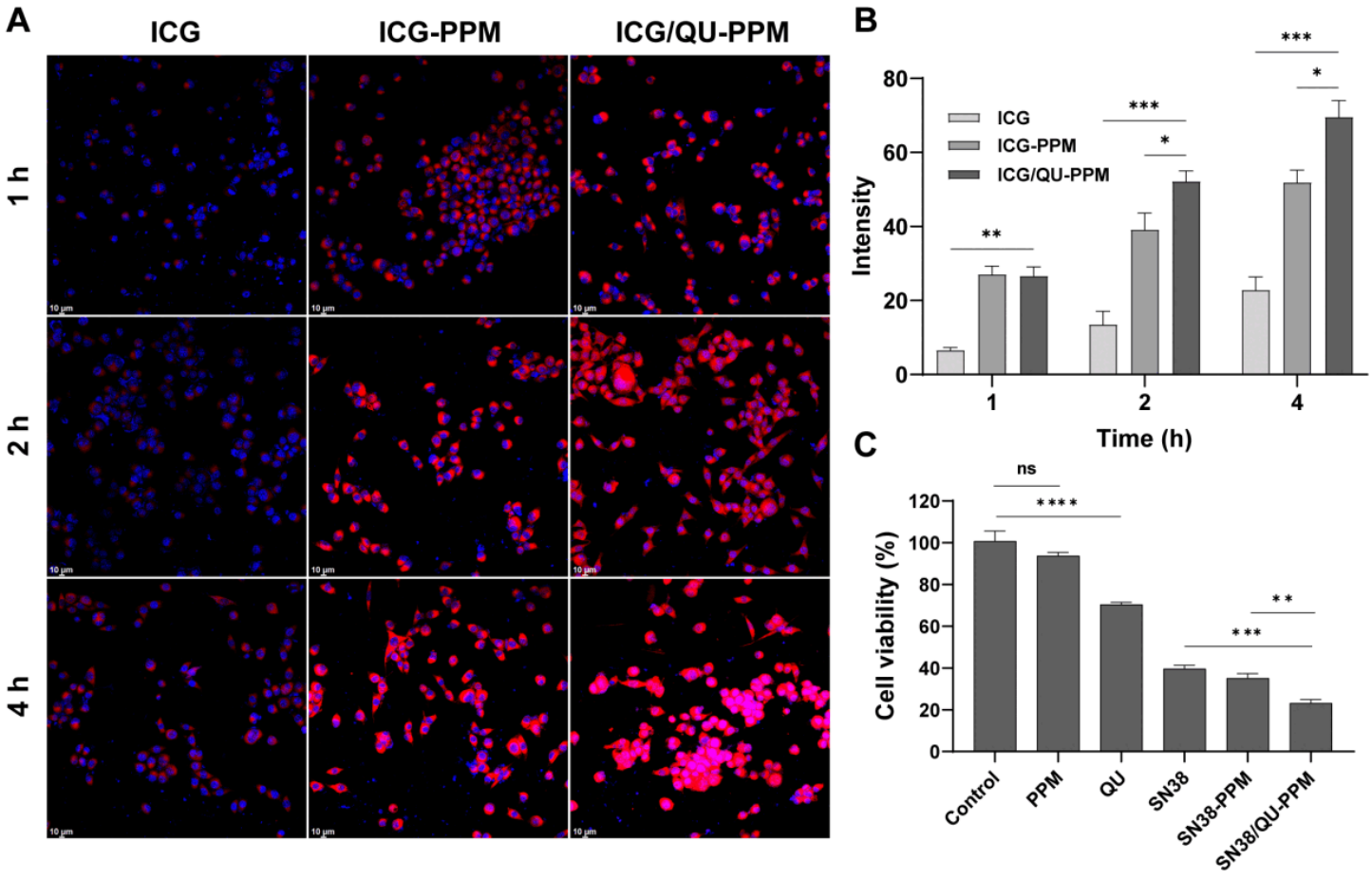


Figure 2

(**A**) CLSM images and (**B**) the corresponding fluorescence quantification of LLC-Luc cells treated with ICG, ICG-PPM or ICG/QU-PPM at different time(n = 3, mean ± SD, *P < 0.05, **P < 0.01 and ***P < 0.001). Scale bar: 10 μm. (**C**) Cell viability of LLC-Luc cells after treatment. (n = 6, mean ± SD, **P < 0.01, ***P < 0.001 and ****P < 0.0001).

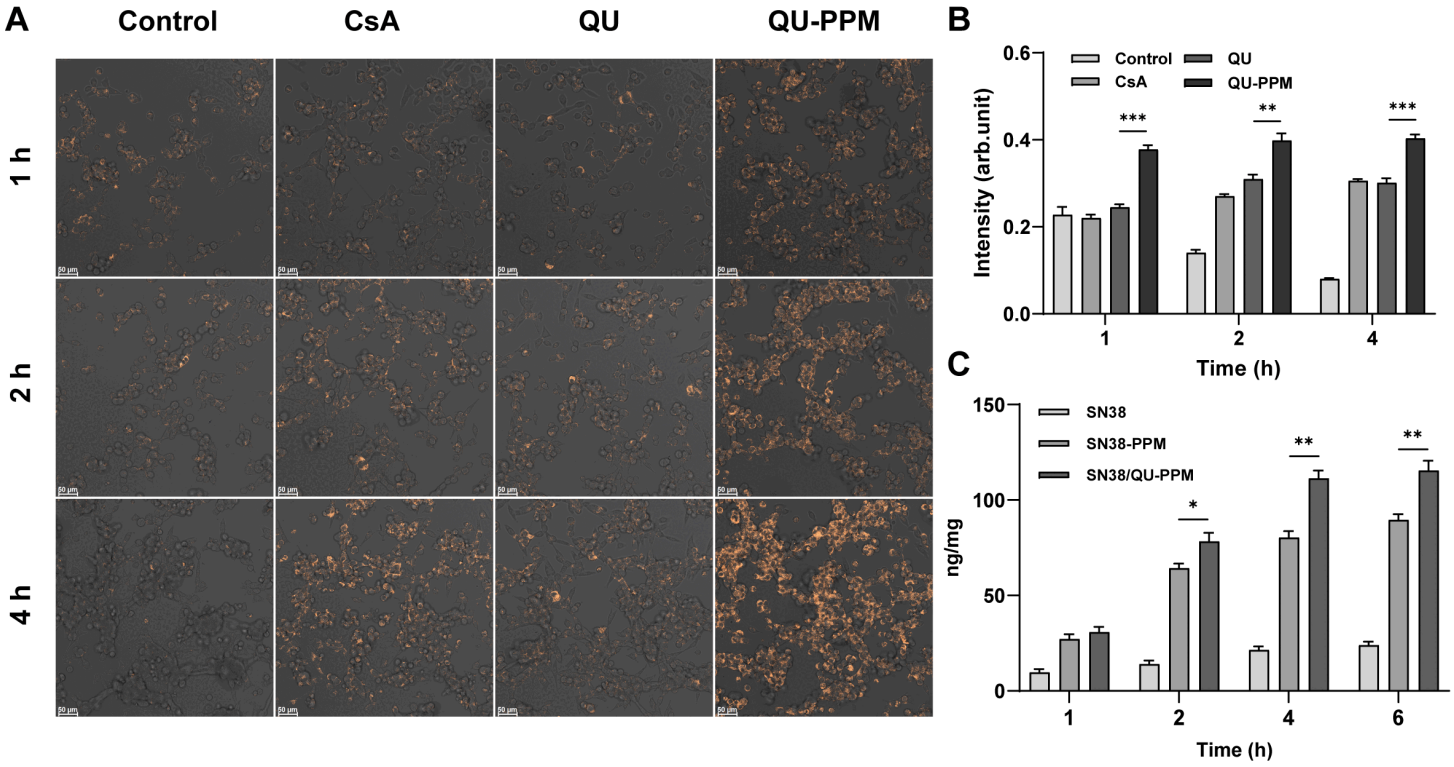


Figure 3

(**A**) CLSM images of THP in LLC-Luc cells after different treatments. Scale bar: 50 μm. (**B**) Quantitative fluorescence evaluation of quercetin-mediated regulation of P-gp function (n = 3, mean ± SD, **P < 0.01, ***P < 0.001). (**C**) Intracellular accumulation of SN38 (n = 3, mean ± SD, *P < 0.05, **P < 0.01).

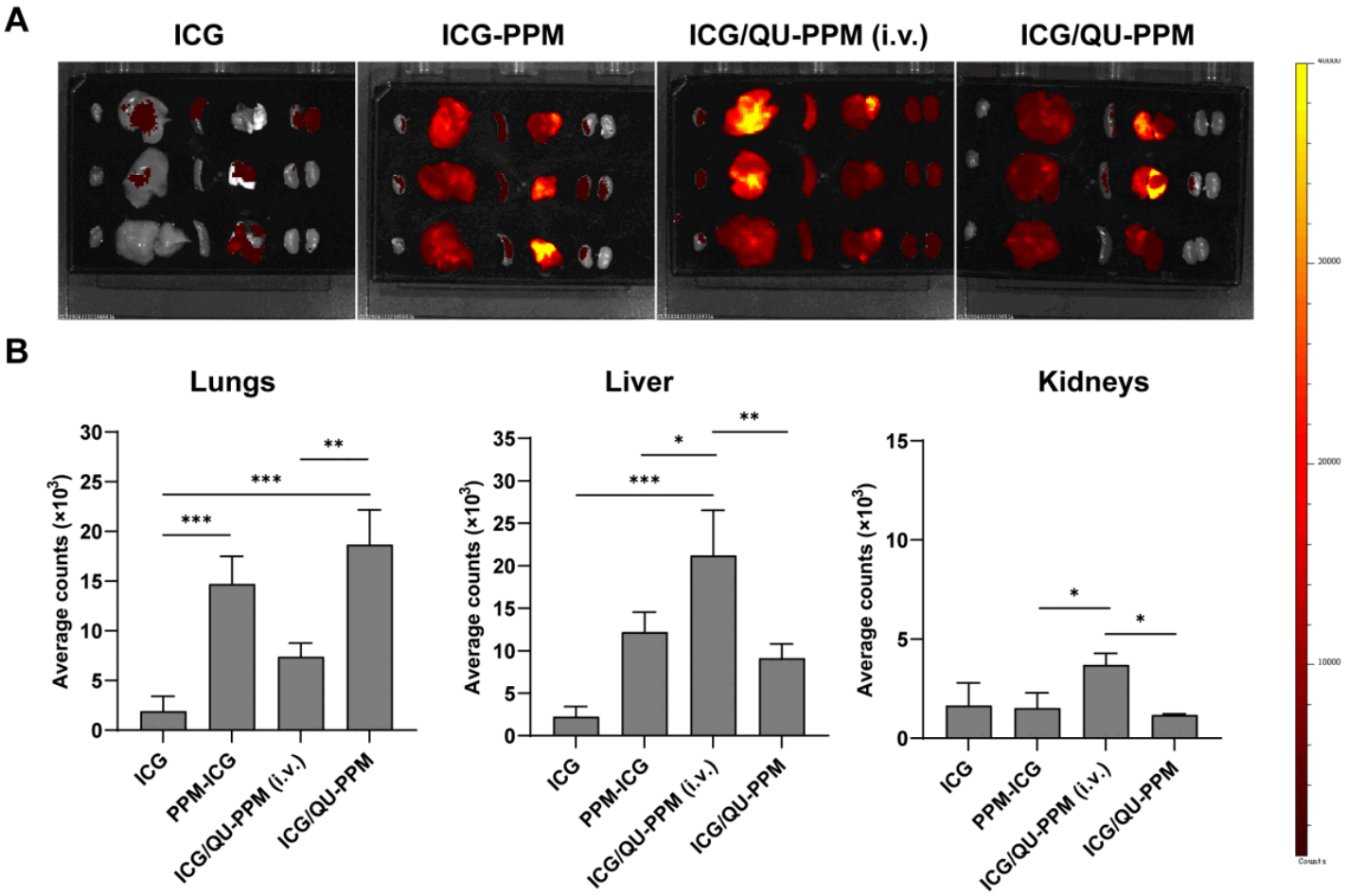


Figure 4

(**A**) Ex vivo fluorescence images of major organs at 24 h after different treatments. (**B**) Quantitative analysis of ex vivo fluorescence intensity (n = 3, mean ± SD, *P < 0.05, **P < 0.01 and ***P < 0.001).

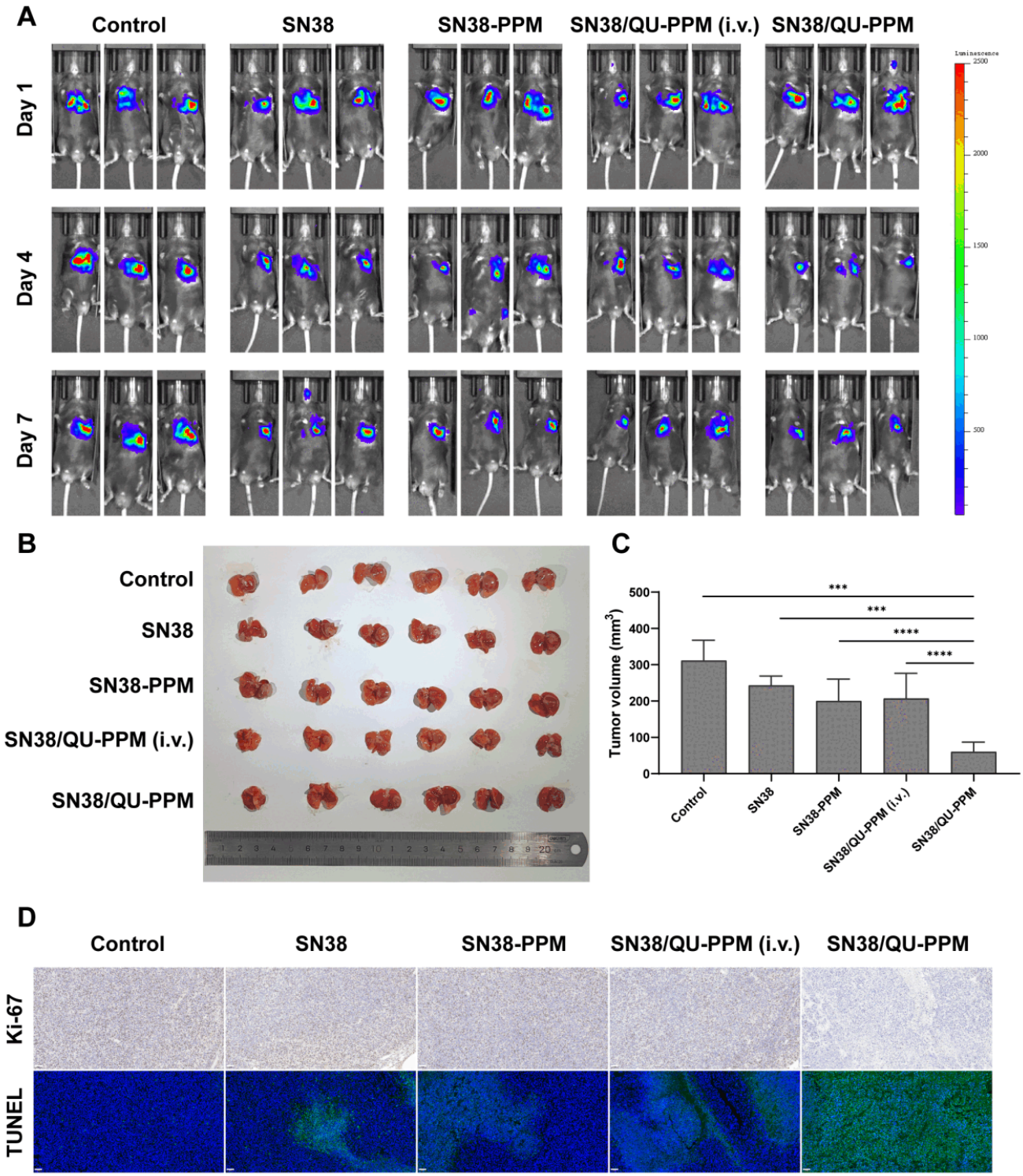


Figure 5

(**A**) Fluorescence imaging of the lungs in orthotopic lung cancer-bearing mice during therapeutic intervention. (**B**) Lung tumor images and (**C**) tumor volume of orthotopic lung cancer-bearing mice acquired via different processing methods (n = 6, mean ± SD, ***P < 0.001 and ****P < 0.0001). (**D**) Ki-67, and TUNEL staining of the tumors. Scale bar = 100 μm.

Supplementary Files

This is a list of supplementary files associated with this preprint. Click to download.

- SupplementaryMaterials.docx